CONF-941144--92

ANALYTICAL ELECTRON MICROSCOPY OF PRECIPITATES IN ION-IMPLANTED $MgAl_2O_4$ SPINEL

N. D. EVANS*, S. J. ZINKLE** AND J. BENTLEY**
*Oak Ridge Institute for Science and Education, PO Box 117, Oak Ridge, TN 37831-0117
**Metals and Ceramics Division, Oak Ridge National Laboratory, PO Box 2008, Oak Ridge, TN 37831-6376

ABSTRACT

Analytical electron microscopy (AEM) has been used to investigate precipitates within $MgAl_2O_4$ spinel following implantation of Al^+, Mg^+, or Fe^{2+} ions. Combined diffraction experiments, energy dispersive X-ray spectrometry (EDS), electron energy-loss spectrometry (EELS), and energy-filtered imaging were employed to identify and characterize precipitates observed in the implanted ion region. Diffraction studies suggested these are metallic aluminum colloids, although EELS and energy-filtered images revealed this to be the case only for the Al^+ and Mg^+ implantations, and not for Fe^{2+} ion implantations. Multiple-least-squares (MLS) fitting of EELS spectra was employed to quantify the volume fraction of metallic aluminum when present in the implanted ion region. Energy-filtered images of the implanted ion region clearly show the colloid distribution in the Al^+ and Mg^+ implanted spinel. Energy-filtered images from the Fe^{2+} ion implanted spinel indicate that the features visible in diffraction contrast cannot be associated with either metallic aluminum or iron-rich precipitates.

INTRODUCTION

Magnesium aluminate spinel ($MgAl_2O_4$) is being considered as an insulator material within proposed fusion reactors where considerable radiation fields are anticipated. Studies have shown this spinel is resistant to both cavity and dislocation loop formation during irradiation to high damage levels [1-4]. Within a study where the relative influence of ionizing and displacive radiation was examined by systematically varying the mass and energy of the bombarding ions, it was noted the microstructure of the irradiated regions, particularly the implanted ion region, is strongly influenced by the injected ions [5]. Nanometer-sized features were observed in the implanted ion region and thought to be metallic aluminum colloids formed due to the chemical effect of the implanted species rather than a damage effect. These features were not observed in the damaged region outside the implanted ion region. The colloids appeared to be in a cube-on-cube orientation relation with the spinel matrix. For this orientation relation, diffraction spots from any aluminum colloids coincide with reflections from spinel because both phases are cubic and the lattice parameter of spinel (0.8083 nm) is almost exactly twice that of aluminum (0.4049 nm); electron diffraction experiments were insufficient for phase identification of these features. Consequently, some specimens from reference [5] have been examined in this AEM study to resolve the identity of these precipitates.

EXPERIMENTAL PROCEDURES

Implantations were performed in the triple ion beam Van de Graaff accelerator facility at Oak Ridge National Laboratory on 3 mm diameter disks of polycrystalline spinel. Specimens were irradiated with 2 MeV Al^+ ions to a fluence of 3.8×21 ions/m^2 [peak damage level of 106 displacements per atom (dpa)] at 923 K, or with 2.4 MeV Mg^+ to a fluence of 2.8×21 ions/m^2 (70 dpa) at room temperature, or with 3.6 MeV Fe^{2+} ions (simultaneously with 1 MeV He^+) to a fluence of 1.1×20 ions/m^2 (10 dpa) at 923 K. Cross-section TEM specimens were prepared by

grinding and dimpling prior to ion milling (6 keV Ar^+ ions) at room temperature until perforation.

Conventional diffraction experiments were performed using a Philips CM12 microscope operating at 120 kV on specimens that were carbon coated to reduce charging. Prior to AEM, specimens were cleaned of carbon by milling (3 keV Ar^+ ions). The EELS was performed in the diffraction mode at 300 kV using a Philips CM30 electron microscope equipped with a Gatan 666 parallel-detection electron energy-loss spectrometer (PEELS). Here, the electron probe was converged to ~200 nm diameter (α~1.5 mrad) and an objective aperture was used to define the collection angle (β~6 mrad). Additional EELS was performed with high spatial resolution using a Philips EM400T/FEG operated at 100 kV and equipped with the aforementioned PEELS. To minimize contamination during spectrometry, a liquid nitrogen cooling holder was used to maintain specimens at ~140 K. Initial experiments in the scanning transmission (STEM) mode with a ~0.8 nA probe of ~2 nm diameter resulted in significant beam damage during spectrum acquisition. Consequently, probes with diameter $\geq$ 50 nm were used in conventional TEM modes for these energy-loss studies. High spatial resolution was achieved in the image mode by positioning at high magnification (100-200 kx) a region or feature-of-interest over the PEELS entrance aperture (α~2 mrad, β~20 mrad). In this setup, areas selected had diameters of ~15 nm. To obtain quantitative profiles of the volume fraction of metallic aluminum within the implanted region, regression analysis was performed on EELS spectra after dark current subtraction and Fourier-log deconvolution [6] to extract single scattering distributions (SSD). Reference spectra used for fitting were obtained from unirradiated spinel and a metallic aluminum specimen. The integrated intensity of the Al K_α peak in hole-count-subtracted EDS analyses was used to normalize EELS reference spectra to identical numbers of aluminum atoms.

Energy-filtered images were obtained using the Philips CM30 with the slow-scan charge coupled device (CCD) camera of a Gatan Imaging Filter (described elsewhere [7]). All acquired images were 512 x 512 pixels in size and gain normalized. Images acquired using zero-loss or low-loss electrons were recorded with 5-eV-wide windows and 1 s exposure times. For images containing contributions from both matrix and colloids (those acquired using 15 eV loss electrons), rudimentary background subtraction of the spinel contribution to the image was accomplished by subtracting one third of the pixel-by-pixel intensity of images acquired at 10 and 20 eV. Additional energy-filtered images were also acquired from the Fe^{2+} ion implanted spinel using core-loss rather than plasmon excitations. Using 30 eV window widths and 15 s exposure times, images were recorded with thresholds at 643 eV (first pre-edge) and 683 eV (second pre-edge) to permit background subtraction by the two area method [8] in images acquired with a threshold at 723 eV (after the Fe $L_{2,3}$ ionization edge).

RESULTS

The <222> reflection from spinel is weak relative to the aluminum <111> reflection. Therefore, the strongly diffracting Nanometer-sized features in the peak damage region of ion implanted spinel, shown in Fig. 1 for $<222>_{sp}/<111>_{Al}$ dark-field images, support the hypothesis that these features are metallic aluminum colloids in a cube-on-cube orientation with the spinel matrix [9].

Additional results from the Al^+ implanted spinel are presented in Figs. 2 to 5. The colloids were differentiated from the spinel matrix via their different volume plasmon losses in EELS. Two spectra, obtained under weakly diffracting conditions, are shown in Fig. 2. Spectrum (a) was acquired with the spinel matrix positioned over the spectrometer entrance aperture; spectrum (b) was acquired with a 10 nm diameter colloid in spinel centered over the entrance aperture. The volume plasmon loss measured from a metallic aluminum specimen is centered at ~15 eV and the valence loss maximum from unimplanted spinel occurs at ~25 eV. The pronounced peak at ~15 eV in spectrum (b) confirms the initial interpretation from dark-field images; the colloids are metallic aluminum. It was assumed that these SSD, acquired from the damaged or implanted regions, contained only contributions from spinel and metallic aluminum. Therefore, quantitative profiles of the volume fraction of metallic aluminum within the implanted region were determined by multivariate linear regression of energy loss spectra [10,11]. Figure 3 shows spectra acquired from (a) unimplanted

DISCLAIMER

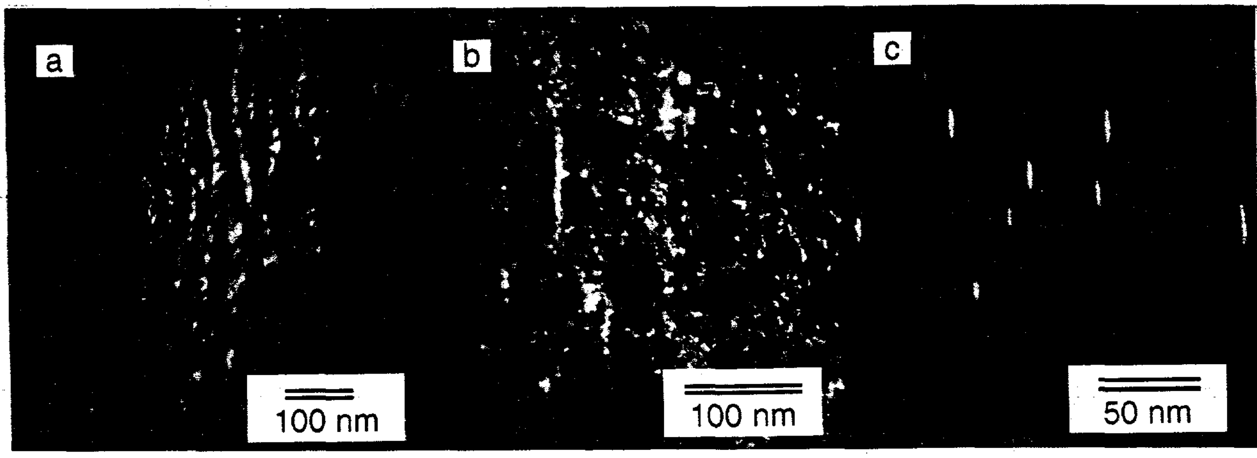

Fig. 1 <222>$_{sp}$ dark field images of implanted ion region in spinel after implantation with (a) Al^+ to 106 dpa, (b) Mg^+ to 70 dpa, (c) Fe^{2+} to 10 dpa.

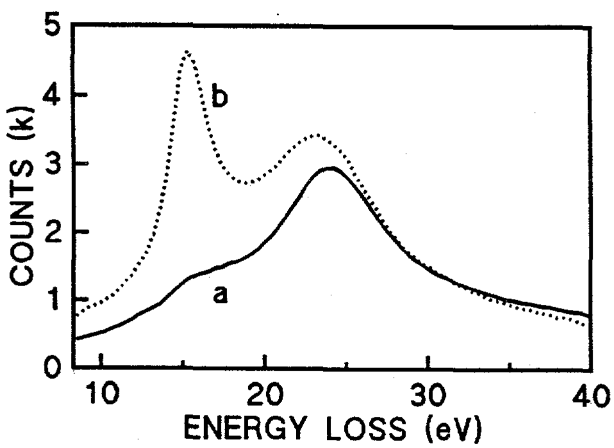

Fig. 2 Volume plasmons from (a) spinel matrix and (b) metallic aluminum colloid.

spinel, (b) metallic aluminum, and (c) the implanted ion region. Spectrum (d) is a weighted summation of spectra (a) and (b) to achieve best-fit with spectrum (c) according to the regression analysis. The regression analysis indicates this region contains 4.5 % metallic aluminum. Similarly, spectra were obtained across the implanted ion region for MLS analysis and the results are shown in Fig. 4. Vertical error bars indicate the 95% confidence intervals about the fitting parameter for the metallic aluminum. The diameters of the large probes used during acquisition of some spectra are indicated by horizontal error bars. There is reasonable agreement between the MLS data for all acquisition schemes and the expected width of the implanted ion profile as calculated from EDEP-1 [12]. The EDEP profile shown has been

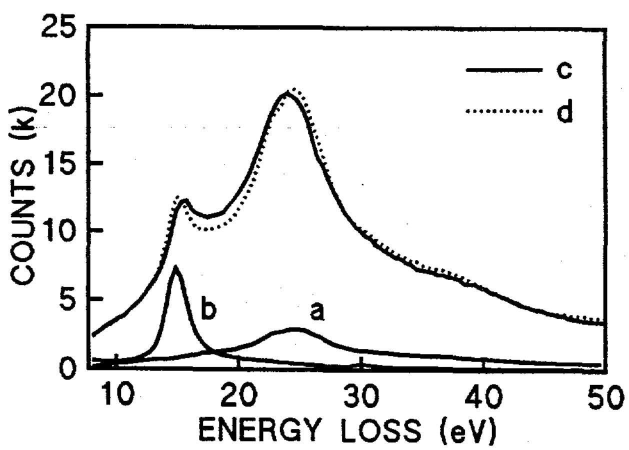

Fig. 3 Plasmon spectra from (a) unimplanted spinel, (b) metallic Al, (c) implanted ion region; (d) composite from regression analysis.

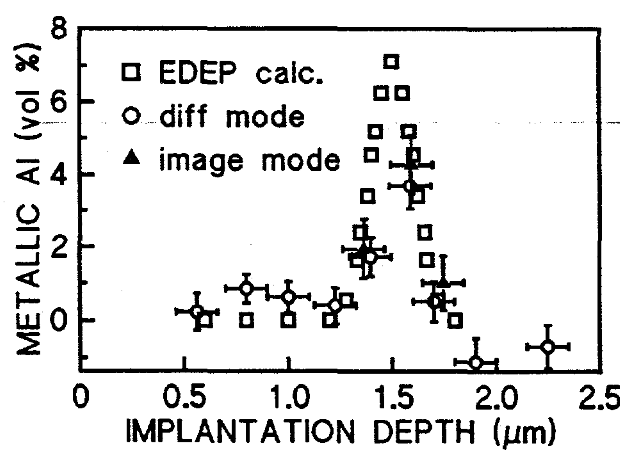

Fig. 4 Quantitative profiles of metallic aluminum within spinel.

artificially shifted to a greater depth (0.2 μm) to make the calculated and measured implanted ion range coincide. Because EELS spectra are acquired in the spinel from regions of different thickness, the spinel surface plasmon impacts the MLS fitting such that an apparent best fit can occur by a reduced metallic aluminum plasmon contribution. This problem is overcome during MLS fitting by use of a spinel reference spectrum from a region similar in thickness to the region being fitted [13].

Energy-filtered bright-field images acquired from the Al^+ implanted spinel are shown in Fig. 5(a-d). The zero-loss image in (a) appears similar to a conventional bright-field image. However, the aluminum colloid distribution is clearly revealed when 15 eV loss electrons are used to produce the image in (b). The image in Fig. 5(c) was produced from 25 eV loss electrons; the light regions correspond to the spinel matrix, and the darker regions, which appear as light regions in (b), are of metallic aluminum. Small colloids, located near the edge of the implanted ion region, have diameters only ~2 nm, as shown in Fig. 5(d) [from 5(b), as indicated]. This clearly demonstrates the utility of

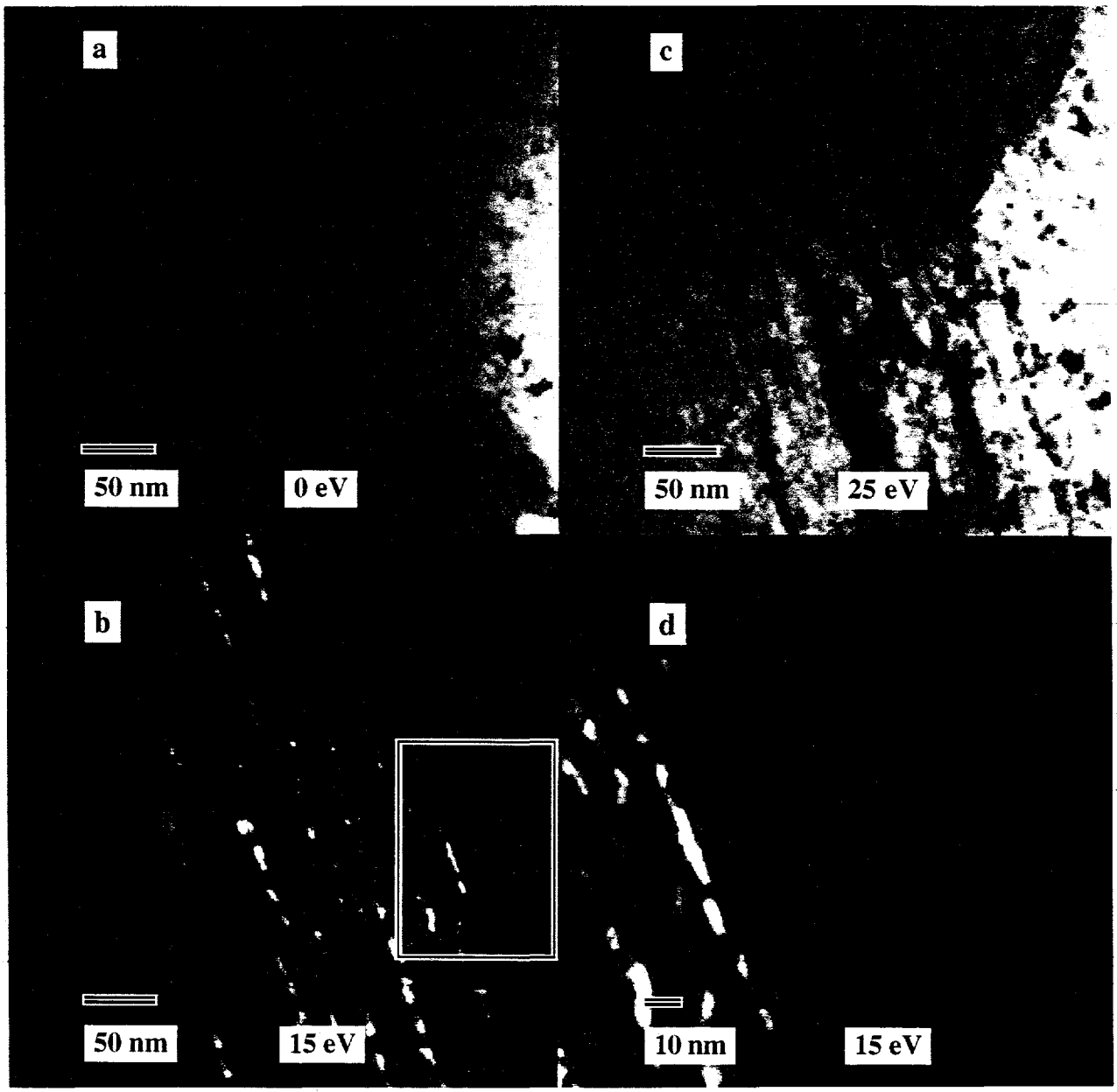

Fig. 5 Energy filtered images of Al^+ implanted spinel (a) elastically scattered zero-loss, (b) Al colloids imaged with 15 eV loss electrons, (c) spinel imaged with 25 eV loss electrons, (d) nanometer-sized colloids revealed at high magnification, 15 eV loss electrons.

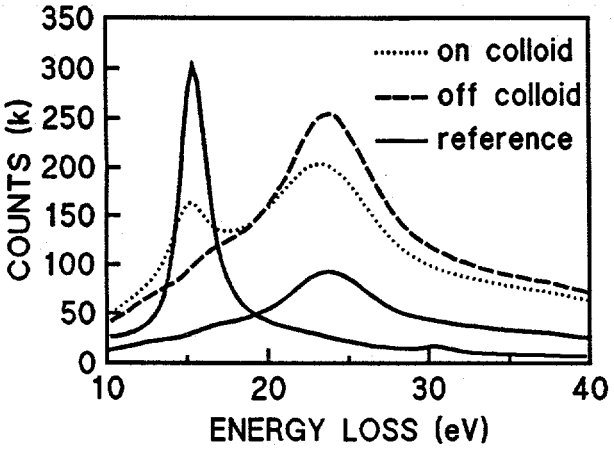

Fig. 6 Mg^+ implantation into spinel produces metallic aluminum colloids.

energy-filtering: very small features, similar to the matrix in chemistry, but having different plasmon spectra, can be imaged in a non-specific diffracting condition.

The spectra acquired from Mg^+ ion implanted spinel indicate the resulting colloids are also metallic aluminum, Fig. 6. A low-loss spectrum acquired from a colloid positioned over the spectrometer entrance aperture shows the distinct volume plasmon of metallic aluminum. Magnesium volume plasmons occur at ~10.5 eV, and plasmon losses in Al-Mg alloys have been measured [14] and do not produce excitations near 15 eV. There is a ~0.3 eV shift to lower energy for the measured plasmon loss relative to the plasmon position from reference material; the shift corresponds to Al-3 at% Mg, indicating the colloids are supersaturated with Mg (equilibrium solubility of Mg in Al at room temperature is ~1 at%). The profile of metallic aluminum measured in the implanted ion range via MLS fitting coincides in both depth and width with a profile of excess Mg measured by EDS. Energy-filtered images using 15 eV loss electrons revealed the presence of metallic aluminum colloids with diameter <2 nm within the implanted ion region, Fig. 7.

Following Fe^{2+} ion implantation, Fe was detected in hole-count-subtracted EDS spectra only in the implanted ion region and not in the near surface region of the implanted spinel. However, only features characteristic of spinel were observed in low-loss spectra acquired from the implanted ion region of this specimen. Energy-filtered images from the Fe^{2+} ion implanted region were obtained to seek both metallic aluminum and regions locally enriched in iron, Fig. 8. The lack of structure in 15 eV loss images [Fig. 8(a)] indicates the diffracting features in Fig. 1(c) are not metallic aluminum colloids. Figure 8(b) is a background subtracted image acquired using Fe $L_{2,3}$ core loss electrons. As no features are present to indicate locally iron-enriched regions, it is unlikely that the diffracting features in Fig. 1(c) are due to agglomerations of pure Fe or an Fe-rich phase, such as an iron oxide. In addition, it is unlikely that the defects are formations of $FeAl_2O_4$ or $MgFe_2O_4$. These iron-enriched spinel phases are cubic as is $MgAl_2O_4$, with similar lattice parameters to $MgAl_2O_4$, and all

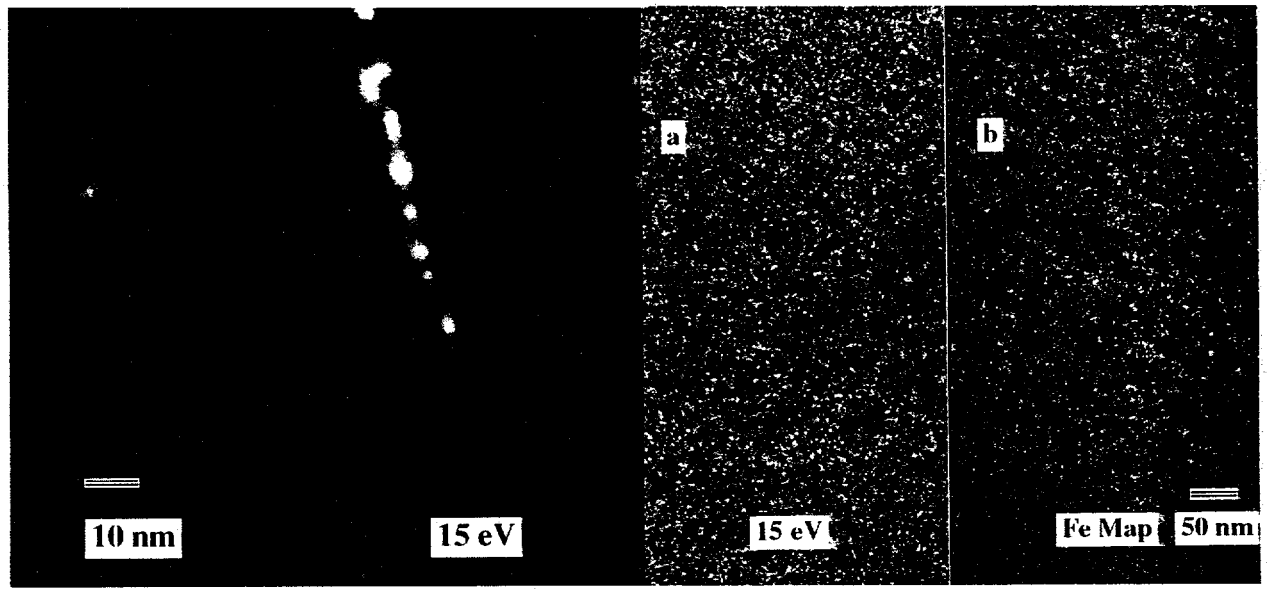

Fig. 7 Metallic Al colloids in Mg^+ ion implanted spinel imaged with 15 eV loss electrons.

Fig. 8 Fe^{2+} ion implanted spinel (a) 15 eV loss electrons, and (b) Fe-$L_{2,3}$ core loss electrons.

three phases have similar (weak) <222> reflections, whereas the defects in Fig. 1(c) are observed due to differences in structure factor.

CONCLUSIONS

Implantation of spinel with Al^+ or Mg^+ ions to 106 and 70 dpa, respectively, leads to the formation of metallic aluminum colloids in the implanted ion region, but not in irradiated regions well separated from the implanted ions. A MLS analysis of plasmon spectra permits the quantification of the metallic aluminum present within the spinel matrix, overcoming difficulties of beam damage due to the use of fine probes. Energy-filtered imaging has successfully mapped Al colloids in $MgAl_2O_4$ spinel with high spatial resolution; ~2 nm diameter features have been observed.

Metallic aluminum colloids were not observed in spinel following Fe^{2+} ion implantation to 10 dpa. Defects visible by diffraction contrast, while seen only in the implanted Fe^{2+} ion region, are not associated with local variations in Fe, within the detection limits of the imaging filter; the identity of these defects remains unknown. Examination of a similar specimen irradiated to a higher fluence of injected iron might reveal the identity of these features as they would likely grow in number and possibly coarsen.

ACKNOWLEDGEMENT

Research sponsored by the Division of Materials Sciences and the Office of Fusion Energy, U.S. Department of Energy, under contract DE-AC05-84OR21400 with Martin Marietta Energy Systems, Inc., and through the SHaRE Program under contract DE-AC05-76OR00033 with Oak Ridge Associated Universities.

REFERENCES

1. F. W. Clinard, Jr., G. F. Hurley, and L. W. Hobbs, J. Nucl. Mater. **108&109**, 655 (1982).
2. C. A. Parker, L. W. Hobbs, K. C. Russell, and F. W. Clinard, Jr., J. Nucl. Mater. **133&134**, 741 (1985).
3. S. J. Zinkle, J. Am. Ceram. Soc. **72**, 1343 (1989).
4. S. J. Zinkle and S. Kojima, Nucl. Instru. Meth. B **46**, 165 (1990).
5. S. J. Zinkle, Nucl. Instr. Meth. B **91**, 234 (1994).
6. R. F. Egerton, Electron Energy-Loss Spectroscopy in the Electron Microscope, (Plenum Press, New York, 1986), p. 229.
7. O. L. Krivanek, A. J. Gubbens, N. Dellby, and C. E. Meyer, Microsc. Microanal. Microstruct. **3**, 187 (1992).
8. ibid., reference 6, p. 257.
9. N. D. Evans, S. J. Zinkle, J. Bentley, and E. A. Kenik, in Proc. 49th Ann. Meet. Electron Microsc. Soc. Amer., G. W. Bailey, and E. L. Hall, eds., (San Francisco Press, San Francisco, 1991), p. 728.
10. A. Romano, Applied Statistics for Science and Industry, (Allyn and Bacon, Inc., Boston, 1977), Chapter 4.
11. P. R. Bevington, Data Reduction and Error Analysis for the Physical Sciences, (McGraw-Hill, New York, 1969), Chapter 5.
12. I. Manning and G. P. Mueller, Comput. Phys. Commun. **7**, 85 (1974).
13. N. D. Evans and Z. L. Wang in Proc. 50th Ann. Meet. Electron Microsc. Soc. Amer., G. W. Bailey, J. Bentley, and J. A. Small, eds., (San Francisco Press, San Francisco, 1992) p. 1256.
14. D. R. Spaulding and A. J. Metherell, Phil. Mag. **18**, 41 (1968).